Very Large Scale Integration of Nano-patterned $YBa_2Cu_3O_{7-\delta}$ Josephson Junctions in a Two-dimensional Array

Shane A. Cybart,[*,†,‡] Steven M. Anton,[†,‡] Stephen M. Wu,[†,‡] John Clarke,[†,‡] and Robert C. Dynes[†,‡]

Department of Physics, University of California, Berkeley, CA, 94720, and Materials Sciences Division, Lawrence Berkeley National Laboratory, Berkeley, CA, 94720

E-mail: scybart@berkeley.edu

Abstract

Very large scale integration of Josephson junctions in a two-dimensional series-parallel array has been achieved by ion irradiating a $YBa_2Cu_3O_{7-\delta}$ film through slits in a nano-fabricated mask created with electron beam lithography and reactive ion etching. The mask consisted of 15,820 high-aspect ratio (20:1), 35-nm wide slits that restricted the irradiation in the film below to form Josephson junctions. Characterizing each parallel segment k, containing 28 junctions, with a single critical current I_{ck} we found a standard deviation in I_{ck} of about 16%.

[†]University of California
[‡]Lawrence Berkeley National Laboratory

In the last two decades there has been considerable effort aimed at developing a high-transition temperature (T_c) superconductor Josephson junction technology capable of producing large numbers of junctions with uniform electrical properties, namely junction critical current I_0 and normal state resistance R_n.[1] This is especially challenging in high-T_c materials compared with conventional metallic low-T_c superconductors because the superconducting coherence length ξ is much shorter and highly anisotropic, typically 2 nm in the *ab* plane and 0.2 nm along the *c*-axis direction.[2] As a result, the superconducting order parameter is susceptible to structural and chemical changes on atomic length scales. Thus very small imperfections in the Josephson barrier or at the interface between the barrier and electrodes can drastically effect I_0, since it depends exponentially on the length of the barrier. Therefore, precise control at the nanometer scale is required to make multiple high-T_c junctions with uniform I_0. High-T_c Josephson devices are further complicated by highly anisotropic electrical transport: conductivity along the *c*-axis is two orders of magnitude smaller than in the *a*-*b* plane.[3] Such anisotropy precludes the possibility of growing epitaxial multilayers to form sandwich type junctions because the highest quality thin films of high-T_c superconductors have *c*-axes orientated normal to the substrate.

Despite these challenges, a number of junction fabrication techniques have emerged. The earliest was to grow a thin film on a bicrystal substrate to create grain boundaries in the superconductor that function as junction barriers.[4] These junctions are used commercially[5,6] in dc superconducting quantum interference devices (SQUIDs), which consist of two junctions connected by a superconducting loop. While successful for small scale applications, these junctions are not suitable for large scale integration because device layout is severely restricted: all the junctions must be located along a single grain boundary. In addition, there are large variations in I_0 and R_n arising from the short YBCO coherence length and imperfections in bicrystal substrates.[7] Another commonly used type of junction is the ramp junction,[8] in which the base junction electrode is milled at an angle and an intermediate barrier material and a superconducting counter electrode are subsequently deposited. Tens of thousands of these junctions have been demonstrated on a single chip,[9–11] and for some applications they show considerable promise for a large scale junction technology.[12,13]

However, they may not be suitable for devices operating at liquid nitrogen temperatures, because the operating temperature is typically below 50 K.[14] Furthermore, the inter-junction spacing can only be scaled down to a few μm,[15] which does not allow them to be used in high frequency devices that may require junction spacings of the order of 100 nm.[16]

An alternative technology is to use ion damage Josephson junctions, which are fabricated by using ion irradiation to reduce T_c[17] in a narrow region of a superconducting bridge. Above the narrow region T_c and below the undamaged electrode T_c, the irradiated area behaves as a Josephson junction. Since ion damage junctions have no interfaces between different materials, they can be arbitrarily positioned, and densely spaced ($\sim$ 100 nm).[18] One way of forming this type of junction is to pattern a thick mask to protect the superconducting electrodes and to damage unmasked regions with ion irradiation. This technique was first demonstrated by Tinchev to fabricate SQUIDs.[19] Others have followed with variations of the process to reproduce single junctions,[20–24] series arrays of tens of junctions,[25,26] and a series array of 280 SQUIDs.[27] Here we report the scaling up of this process by two orders of magnitude, with a 2-dimensional (2D) array of 15,820 (28×565) Josephson junctions or equivalently 15,255 (27×565) SQUIDs.

We designed a SQUID configuration with incommensurate loop areas because of recent significant interest in these structures. The critical currents of each SQUID oscillate with incommensurate periodicities as a function of applied magnetic field B. As a result, the critical current of the entire array I_{ca} attains a maximum value at zero magnetic field, but is nearly zero elsewhere. Consequently, for Josephson junctions with nonhysteretic current-voltage (I-V) characteristics, the array biased with a (negative) current exhibits a sharp peak in voltage at zero field. This behavior was first demonstrated by Sohn *et al.*[28] using 2D arrays of Nb-AlO_x-Nb Josephson junctions. Later Carelli *et al.*[29] showed that one could use a series array of incommensurate area SQUIDs as an absolute magnetometer. More recently, arrays of incommensurate area SQUIDs made from the high-T_c superconductor $YBa_2Cu_3O_{7-\delta}$ (YBCO) have been fabricated with loops connected in series, parallel, and a series-parallel combination.[30,31] It has been suggested that it may be possible to use incommensurate area SQUID arrays as radio frequency (RF) amplifiers.[32]

The layout of our array is shown in Figure 1. For efficient coupling of RF in future experiments we chose a microstrip line configuration with SQUID loops cut into it. The following criteria were used in designing this array. The width of the microstrip was set to be 500 μm so that its impedance would be 50 Ω on a 0.5-mm thick sapphire substrate. The junction widths were chosen to be 2 μm to avoid self-field-limited junction effects[33] and to keep R_n high. The parameter $\beta_L \equiv 2LI_0/\Phi_0$ (where L is the loop inductance and Φ_0 is the flux quantum) was kept small ($\beta_L < 0.05$) to ensure that $I_{ca}(B)$ modulates almost to zero.[34] This was achieved by using loop areas < 90 μm^2 to keep $L \leq 53$ pH. The overall length of the array in the direction of the bias current was chosen to be 3 mm, less than $1/4$ wavelength for frequencies below 10 GHz, so that the array behaves as a lumped element. The 500-μm width of the microstrip enabled us to fit 27 loops, connected in parallel, across it (Figure 1). The widths of these loops ranged from 9.5 to 22.5 μm in 0.5-μm increments. In the direction of the current, 565 parallel segments with lengths ranging from 3.0 to 4.0 μm in 0.25-μm increments were connected in series in 113 blocks of five.

To create this array, a 200-nm thick YBCO thin film[35] was thermally coevaporated on a sapphire wafer followed by a gold contact layer deposited *in situ*. We patterned the films using photolithography and Ar^+ ion milling to fabricate the microstrip with 15,255 SQUID loops etched into it (Figure 2a). The gold layer over the junctions was removed using a subsequent photolithography step and Transene chemical gold etch, leaving the contact pads (shown in Figure 1). The next step was to fabricate the junctions. The wafer was coated with a 700-nm layer of Shipley S1808 hard-baked photoresist that served as the main ion stopping layer. A 25-nm layer of germanium was electron-beam evaporated on top of the resist and served as an etch stop. We next spun 100 nm of polymethylmethacrylate (PMMA) resist on to the Ge for electron-beam lithographic patterning (Figure 2b). Using a 100-keV Leica VB6-HR nanowriter, we wrote 35-nm wide lines in the PMMA over the locations intended for the junctions. This pattern was transferred into the Ge layer with reactive ion etching (RIE) in a HBr-Cl_2 plasma. The pattern in the Ge was transferred to the resist using low temperature (-100°C), low pressure (5 mtorr) oxygen RIE (Figure 2c). This process resulted in a high aspect ratio of the line width to the trench depth (1:20) because resist

etches two orders of magnitude faster then Ge in an oxygen plasma.

Figure 3a shows a scanning electron microscope (SEM) image of a section of the structure after etching and before implantation. The image was taken using an 18-kV acceleration voltage that partially penetrated the mask and allowed for simultaneous imaging of both the top of the mask and the YBCO film below. A magnified view of two junction regions (Figure 3b) shows the 5-μm long, 35-nm wide slits patterned into the mask. The etches were checked for undercutting by simultaneously processing a silicon dummy wafer with the same layered structure. This test wafer was cleaved, and the cross-sectional image is shown in Figure 3c. Following etching, the wafers were implanted commercially with 200-keV Ne^+ at a dose of $1x10^{13}$ ions/cm^2. The T_c of the YBCO not protected by the mask was lowered by ion damage, forming planar inline Josephson junctions.

Completed devices were attached to a printed circuit board equipped with π-filters and a silicon diode thermometer. The board was mounted inside a vacuum probe and cooled in a liquid nitrogen bath. We measured the resistance of the device as a function of decreasing temperature using a lock-in amplifier and a 22-Hz, 8-μA peak current. As shown in Figure 4, the device exhibited two distinct superconducting transitions: one for the undamaged YBCO and another for the ion damaged material (junctions). The transition temperatures were 86.3 ± 0.2 K and 78.7 ± 0.2 K, where we defined each transition temperature to correspond to the point of inflection in the R vs. T characteristic, or equivalently to the peaks in dR/dT vs. T. Thus, the ion damage reduced T_c by about 7.6 K. The full-width at half maximum (FWHM) for the dR/dT peak of the irradiated material, 1.4 ± 0.2 K, was similar to that of the electrodes, 1.3 ± 0.2 K. Thus, the spread in the T_c of the junctions in the 565 segments in series is close to the spread in the T_c of the unirradiated YBCO. This implies that the spread in T_c along each parallel segment is likely to be comparable. These measurements suggest that the ion damage is quite uniform across the array, implying that the resistances of the weak links are similarly uniform. We note that we previously observed a similar spread in the T_c of a 1D array of 280 SQUIDS.[27]

We measured I-V characteristics for the array; data for five representative temperatures are

shown in Figure 5. To fit the characteristics, we made three initial assumptions. First, we assumed that each parallel segment has a resistance of $R/565$, where $R(T)$ is the fitted resistance of the total array at each temperature. Second we assumed that each parallel segment k of the array behaves as a single, resistively shunted junction[36,37] with a critical current I_{ck}. Third, we assumed that the set of I_{ck} have a normal distribution given by $I_{ck} = \bar{I}_c(1+\delta_k)$, where $\bar{I}_c$ is the mean critical current of the parallel segments and δ_k is the fractional variation in the critical current I_{ck} of segment k. Under these assumptions, we fitted the data using a nonlinear regression with $V = (R/565)\sum_{k=1}^{565}(I^2 - I_{ck}^2)^{1/2}$ $(I > I_{ck})$ to find $\bar{I}_c$, and the standard deviation in I_c, $\sigma(I_c)$. We found that $\sigma(I_c)$ converges to about 16% with decreasing temperature. At higher temperatures thermal noise rounding[38] of the I-V characteristic was indistinguishable from spreads in I_c. In the inset of Figure 5, we see that the resistance determined from the fit increases rapidly with increasing temperature. The solid line linear fit shows that $\bar{I}_c$ scales as $(1-T/T_c)^3$, consistent with a soft boundary model of ion damage junctions near T_c.[39] We remark that in this 2D array the parallel segments enable us to operate with a lower critical current in each junction and retain phase coherence closer to T_c where the soft boundary model[39] is applicable. In our previous work on a one-dimensional series array[27] the need to achieve phase coherence required us to work further below T_c where the critical current scales as $(1-T/T_c)^2$. We found that $T(\bar{I}_c)$=78.3 K for $\bar{I}_c$ = 8 μA, in good agreement with the transition temperature found from Figure 4 at the bias current of 8 μA used for that measurement.

To study the response of the array to a magnetic field, the array was biased with a static (negative) current and the voltage across the array was measured as a function of applied magnetic field. Three different field scales are shown in Figure 6. For large fields (Figure 6a) the Fraunhofer diffraction pattern (approximately $|\mathrm{sinc}\,(\pi\Phi/\Phi_0)|$) from the areas of the individual junctions is observed. Five oscillations are visible, indicating that the junction areas have good uniformity. From the period in the Fraunhofer pattern we calculate the YBCO penetration depth to be 480 nm at 77.3 K. The hysteresis in the data arises from vortex trapping that depends on the magnetic field sweep direction and magnitude.[40] For intermediate fields (Figure 6b) both the Fraunhofer and SQUID pattern are visible. Detailed measurements near $B = 0$, for 6 different bias currents, are

shown in Figure 6c. The central peak is observed at 38 μT. This is where our applied field cancels the component of Earth's field perpendicular to the plane of the array leaving it in zero absolute field. Away from the peak, the oscillations diminish as a result of destructive interference due to the different loop sizes. We performed simulations to characterize the width of the central voltage peak, ΔB, which we define as the separation of the minima on either side. From Figure 6c, we find ΔB = 20.5 $\pm$ 0.5 T. We inserted the areas of the SQUIDs and the fitted parameters $\bar{I}_c$ and R into Eq. (14) of Oppenländer *et al.*[41] The results of the simulations greatly underestimated the width of the peak. We found, however, that a modified model, in which the 27 x 5 block of SQUIDs was modeled by a 1D series array of 5 SQUIDs each with areas corresponding to the average areas of the parallel segments (48, 52, 56, 60, 64 μm^2), predicted ΔB = 20.9 T, about 2% greater than the measured value. We have no ready explanation for this empirical result.

We also observe a linear tilt in V vs. B, visible in Figure 6c, that we ascribe to the motion of Josephson vortices in the array. This motion is analogous to the motion of Abrikosov vortices in type II superconductors. Here, the bias current exerts a Lorentz force given by $(\overrightarrow{J} \times \overrightarrow{B})$ where $\overrightarrow{J}$ is the current density and $\overrightarrow{B}$ is the magnetic field. This force causes vortices to drift with a steady velocity across the array, creating an electric field in the direction of the bias current. On our measurements this appeared as magnetoresistance. For bias currents in the opposite direction, the asymmetry had the opposite sign, consistent with our interpretation. We analyzed our data using the Bardeen-Stephen equation[42] $\rho = \Phi_0 B/\eta B$, which relates the flow resistivity ρ to the magnetic field B, to determine η, the vortex viscosity coefficient. Using the bias current and junction geometrical parameters we converted V to ρ, and determined $\Phi_0 B/\eta$ from a linear fit of the data. We estimate $\eta = 3 \times 10^{-7}$ kg m^{-1}s^{-1} at a current bias of 100 μA. We are not aware of any other measurements of Josephson vortex motion in 2D arrays of this type for comparison. However this value is typical for the viscosity coefficient of Abrikosov vortices in high-transition temperature superconductors.

In conclusion, by building an array of 15,820 Josephson junctions, we have demonstrated that it is possible to fabricate large numbers of ion damage high-T_c Josephson junctions with uniform

properties over large areas. This technique shows promise for a very large scale junction technology. In particular, the relatively small standard deviation (16%) in I_{ck} implies that long, linear arrays containing parallel segments of equal-area SQUIDs have substantial potential for applications such as magnetometers and amplifiers. Since the flux-to-voltage transfer coefficient scales as N, the number of SQUIDS,[43] and the signal-to-noise-ratio scales as $N^{1/2}$, such arrays are likely to overcome the low transfer coefficient and signal-to-noise ratio associated with the low junction resistance inherent in this technology. Furthermore, smaller barrier dimensions combined with narrower bridges made with refinements in lithography and/or new techniques involving nano-wires[44] may allow for substantial increases in I_0R_n, opening up this process to more applications such as rapid single flux quantum logic or precision digital-to-analog conversion.

Acknowledgement

The authors thank Bruce Harteneck for the electron-beam lithography and RIE performed at the LBNL Molecular Foundry, and Yen-Hao Chen for circuit board layout. This work was supported by AFOSR Grant No. FA9550-05-1-0436. The work at the Molecular Foundry and electrical transport measurements were supported by the Office of Science and Office of Basic Energy Sciences of the U.S. Department of Energy under Contract No. DE-AC02-05CH11231.

References

(1) Koelle, D.; Kleiner, R.; Ludwig, F.; Dantsker, E.; Clarke, J. Rev. Mod. Phys. **1999**, 71, 631–686.

(2) Worthington, T.; Gallagher, W.; Dinger, T. Phys. Rev. Lett. **1987**, 59, 1160–1163.

(3) Friedmann, T.; Rabin, M.; Giapintzakis, J.; Rice, J.; Ginsberg, D. Phys. Rev. B **1988**, 42, 6217.

(4) Chaudhari, P.; Mannhart, J.; Dimos, D.; Tsuei, C. C.; Chi, J.; Oprysko, M. M.; Scheuermann, M. Phys. Rev. Lett. **1988**, 60, 1653–1656.

(5) STAR Cryoelectronics, 25-A Bisbee Court, Santa Fe, NM 87508-1412.

(6) Supracon AG, Wildenbruchstr.15, 07745 Jena, Germany.

(7) McDaniel, E. B.; Gausepohl, S. C.; Li, C.-T.; Lee, M.; Hsu, J. W. P.; Rao, R. A.; Eom, C. B. Appl. Phys. Lett. **1997**, 70, 1882–1884.

(8) Gao, J.; Aarnink, W.; Gerritsma, G.; Rogalla, H. Physica. C. **1990**, 171, 126–130.

(9) Martens, J. S.; Pance, A.; Char, K.; Lee, L.; Whiteley, S.; Hietala, V. M. Appl. Phys. Lett. **1993**, 63, 1681–1683.

(10) Burkhardt, H.; Brugmann, O.; Rauther, A.; Schnell, F.; Schilling, M. IEEE. Trans. Appl. Supercond. **1999**, 9, 3153–3156.

(11) Wakana, H.; Adachi, S.; Kamitani, A.; Nakayama, K.; Ishimaru, Y.; Tarutani, Y.; Tanabe, K. IEICE Trans. Electron. **2005**, 208–215.

(12) Wakana, H.; Adachi, S.; Kamitani, A.; Nakayama, K.; Ishimaru, Y.; Oshikubo, Y.; Tarutani, Y.; Tanabe, K. IEEE. Trans. Appl. Supercond. **2005**, 15, 153–156.

(13) Hunt, B.; Forrester, M.; Talvacchio, J. In Engineering Superconductivity; Lee, P., Ed.; Wiley-VCH, 2001; pp 248–259.

(14) Tanabe, K.; Hidaka, M. IEEE. Trans. Appl. Supercond. **2007**, 17, 494–499.

(15) Murduck, J.; Talvacchio, J.; Kahler, D.; Kirschenbaum, A.; Miller, D. http://sensor.northgrum.com/es/stc/cryo/areas/abstract/asc03jmm.pdf **2003**.

(16) Benz, S. P.; Dresselhaus, P. D.; Burrough, C. J. IEEE. Trans. Instrum. Meas. **2001**, 50, 1513–1518.

(17) M.Valles, J.; White, A. E.; Short, K. T.; Dynes, R. C.; Garno, J. P.; Levi, A. F. J.; Anzlowar, M.; Baldwin, K. Phys. Rev. B. **1989**, 39, 11599–11602.

(18) Chen, K.; Cybart, S. A.; Dynes, R. C. IEEE. Trans. Appl. Supercond. **2005**, 15, 149–152.

(19) Tinchev, S. S. Supercond. Sci. Technol. **1990**, 3, 500503.

(20) Simon, R.; Bulman, J.; Burch, J.; Coons, S.; Daly, K.; Dozier, W.; Hu, R.; Lee, A.; Luine, J.; Platt, C. et al. IEEE Trans. Magn. **1991**, 27, 3209–3214.

(21) Barth, R.; Hamidi, A. H.; Hadam, B.; Hollkott, J.; Dunkmann, D.; Auge, J.; Kurz, H. Microelectr. Eng. **1996**, 30, 407–410.

(22) Katz, A. S.; Sun, A. G.; Woods, S. I.; Dynes, R. C. Appl. Phys. Lett. **1998**, 72, 2032–2034.

(23) Kang, D.-J.; Burnell, G.; Lloyd, S. J.; Speaks, R. S.; Peng, N. H.; Jeynes, C.; Webb, R.; Yun, J. H.; Moon, S. H.; Oh, B.; Tarte, E. J.; Moore, D. F.; Blamire, M. G. Appl. Phys. Lett. **2002**, 80, 814–816.

(24) Bergeal, N.; Grison, X.; Lesueur, J.; Faini, G.; Aprili, M.; Contour, J. P. Appl. Phys. Lett. **2005**, 87, 102502.

(25) Chen, K.; Cybart, S. A.; Dynes, R. C. Appl. Phys. Lett. **2004**, 85, 2863–2866.

(26) Cybart, S. A.; Chen, K.; Dynes, R. C. IEEE. Trans. Appl. Supercond. **2005**, 15, 241–244.

(27) Cybart, S. A.; Wu, S. M.; Anton, S. M.; Siddiqi, I.; Clarke, J.; Dynes, R. C. Appl. Phys. Lett. **2008**, 93, 182502.

(28) Sohn, L. L.; Tuominen, M. T.; Rzchowski, M. S.; Free, J. U.; Tinkham, M. Phys. Rev. B **1993**, 47, 975.

(29) Carelli, P.; Castellano, M. G.; Flacco, K.; Leoni, R.; Torrioli, G. Europhys. Lett. **1997**, 39, 569–574.

(30) Schultze, V.; Ijsselsteijn, R.; Meyer, H. G.; Oppenlander, J.; Haussler, C.; Schopohl, N. IEEE. Trans. Appl. Supercond. **2003**, 13, 775–778.

(31) Caputo, P.; Oppenlander, J.; Haussler, C.; Tomes, J.; Friesch, A.; Trauble, T.; Schopohl, N. Appl. Phys. Lett. **2004**, 85, 1389–1391.

(32) Kornev, V. K.; Soloviev, I.; Klenov, N. V.; Mukhanov, O. A. IEEE. Trans. Appl. Supercond. **2007**, 17, 569–572.

(33) Owen, C.; Scalapino, D. Phys. Rev. **1967**, 164, 538–544.

(34) Tesche, C.; Clarke, J. J. Low Temp. Phys. **1977**, 29, 301–331.

(35) Purchased from Theva Dünnschichttechnik GmbH, Rote-Kreuz-Str. 8, D-85737 Ismaning Germany.

(36) McCumber, D. J. Appl. Phys. **1968**, 39, 3113.

(37) Stewart, W. C. Appl. Phys. Lett. **1968**, 12, 277–280.

(38) Ambegaokar, V.; Halperin, B. I. Phys. Rev. Lett. **1969**, 22, 1364–1366.

(39) Katz, A. S.; Woods, S. I.; Dynes, R. C. J. Appl. Phys. **2000**, 87, 2978–2983.

(40) Bean, C. P. Rev. Mod. Phys. **1964**, 36, 31–39.

(41) Oppenländer, J.; Häussler, C.; Schopohl, N. Phys. Rev. B **2000**, 63, 024511.

(42) Bardeen, J.; Stephen, M. J. Phys. Rev **1965**, 140, A1197.

(43) Welty, R. P.; Martinis, J. M. IEEE Trans. Magn. **1991**, 27, 2924–2926.

(44) Xu, K.; Heath, J. R. Nano Lett. **2008**, 8, 3845–3849.

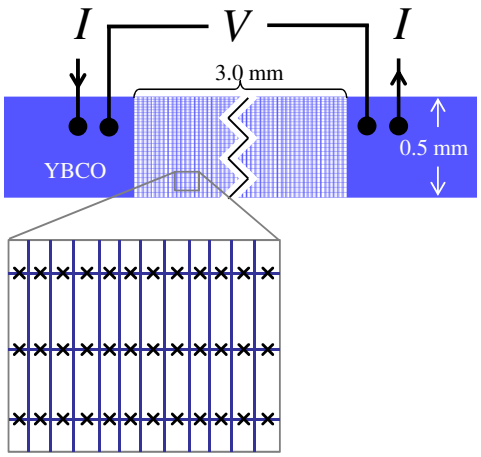

Figure 1: Layout of a 2D array of SQUIDs patterned as a microstrip. The array has 565 series segments of 28 Josephson junctions connected in parallel. Junctions are represented by an $\times$.

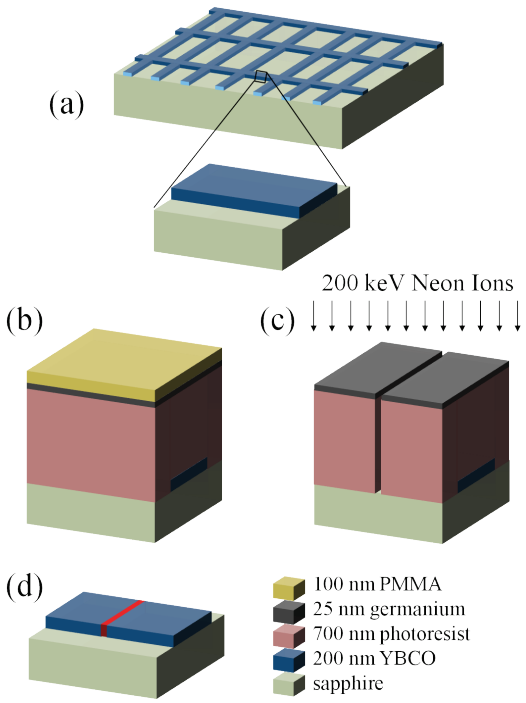

Figure 2: Fabrication process for ion damage Josephson junctions. (a) Magnified view of a patterned YBCO bridge. (b) Layered structure of photoresist, germanium and PMMA. (c) Structure after EBL, RIE and during irradiation. (d) YBCO with reduced T_c shown in red.

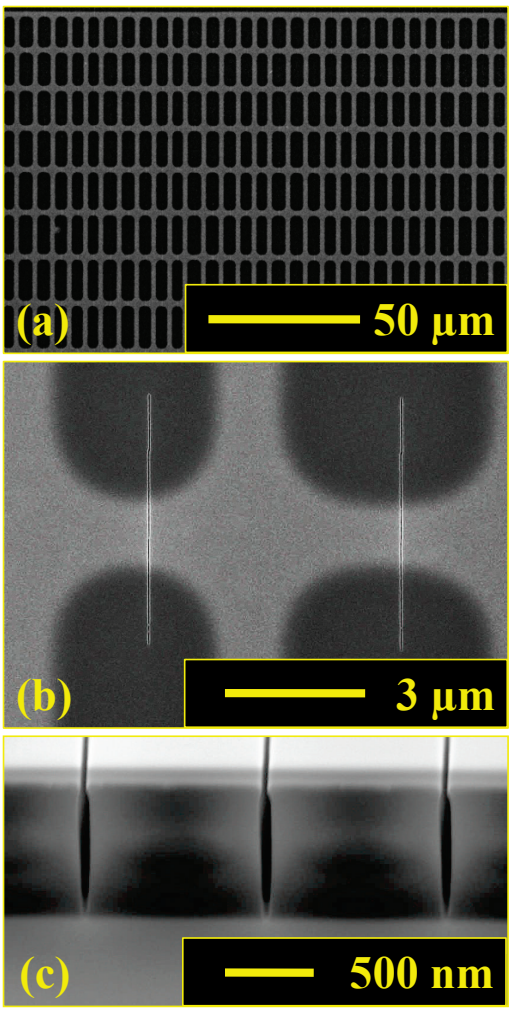

Figure 3: SEM photographs after RIE etching of the implant mask. (a) A segment of the device showing some of the YBCO loops. (b) Magnified view over two of the slits that were used to pattern the junctions. (c) Cross-sectional view of a dummy sample to test the RIE etch for undercutting and to ensure that the etching was complete.

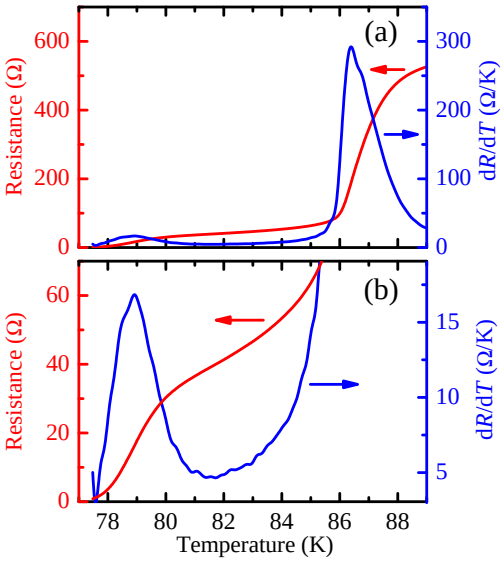

Figure 4: Resistance R and $\mathrm{d}R/\mathrm{d}T$ vs. temperature. (a) Transitions of the electrodes and weak links. (b) Transition of the weak links shown on an expanded scale. The width of the peak in $\mathrm{d}R/\mathrm{d}T$ at each transition gives a measure of the homogeneity of T_c of the electrodes and weak links.

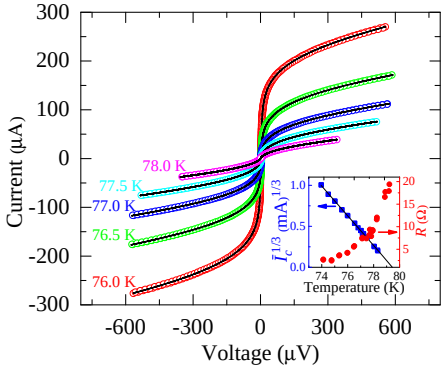

Figure 5: I-V characteristics for 5 temperatures for the 2D Josephson array showing both data (circles) and fitted results (solid lines). The inset shows fitted R vs. T(red) and $\bar{I}_c{}^{1/3}$ vs. T(blue).

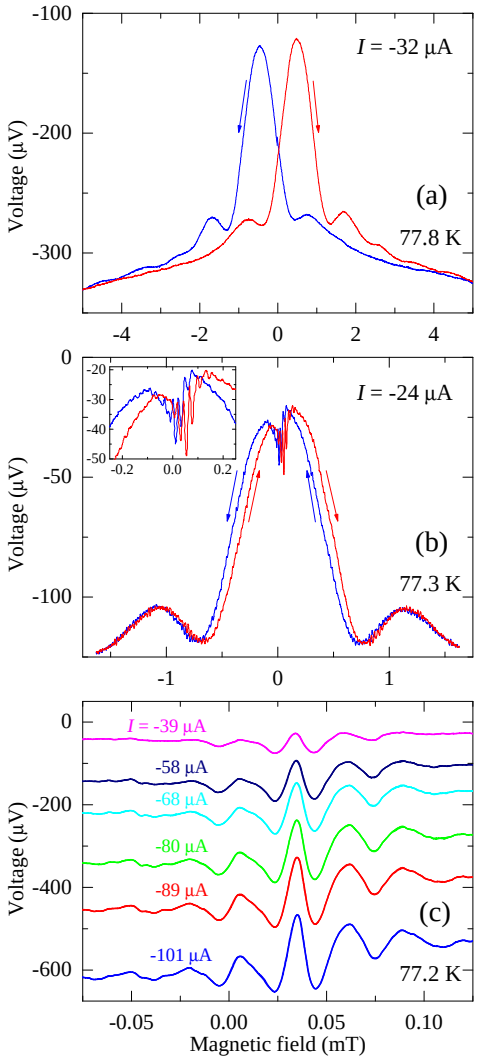

Figure 6: Voltage as a function of magnetic field for (a) large , (b) medium, and (c) small field ranges. The smallest range shows measurements for six bias currents.